THE JOURNAL OF PHYSICAL CHEMISTRY B

Article

Quantum and Classical Molecular Dynamics Simulations of Hydrophobic Hydration Structure around Small Solutes

Jeffrey C. Grossman, Eric Schwegler, and Giulia Galli

J. Phys. Chem. B, **2004**, 108 (40), 15865-15872 • DOI: 10.1021/jp0470187

Quantum and Classical Molecular Dynamics Simulations of Hydrophobic Hydration Structure around Small Solutes

Jeffrey C. Grossman,* Eric Schwegler, and Giulia Galli

Lawrence Livermore National Laboratory, 7000 East Avenue, Livermore, California 94550

Received: July 6, 2004; In Final Form: July 22, 2004

We present a combination of classical and first principles molecular dynamics simulations of hydrophobic hydration structure. Our results show that water molecules surrounding two small hydrophobic solutes are oriented in a similar fashion, and that the driving force for this orientation is the water−water interaction rather than the water−solute interaction. In contrast, the spatial distribution of water around the hydrophobic solute is strongly influenced by the solute, and the driving force for the observed distribution is largely a steric effect. In addition to the size and structure of the solute, we find that the spatial distribution of water is sensitive to pressure. Using quantum simulations as a benchmark for classical potentials, we evaluate the accuracy of several empirical based models in predicting detailed information regarding the structure of water around small hydrophobic solutes. Our results demonstrate that the radial and spatial distribution of water molecules around different solutes obtained classically and quantum mechanically agree rather well, indicating that classical potentials are well suited for examining these properties related to hydrophobic hydration structure. However, we do find that properties such as the angular distribution of water and hydrogen bond ring statistics agree to a lesser extent and depend strongly on the classical potential employed.

I. Introduction

The hydrophobic effect plays a central role in processes spanning numerous scientific and technological disciplines, from protein folding[1] to the formation of natural gas hydrates in oil and gas pipelines.[2] Considerable experimental research has focused on understanding the thermodynamic properties that govern the hydrophobic effect, particularly since the discovery that thermal features of protein denaturization resemble those for transferring small nonpolar molecules to water.[1,3] Advances in experimental techniques have provided insight into the structural nature of water around hydrophobic solutes.[4−10] However, few experiments have measured the arrangement of water *at the molecular level* in response to a hydrophobic solute because probing an interface only several molecules thick poses an enormous challenge. Theoretical work has been limited so far to empirical models,[11−19] which have made numerous important contributions to the understanding of hydrophobic hydration. Yet, it is important to gauge the accuracy of these classical potentials in describing hydrophobic hydration structure, particularly given the weak electrostatic interactions involved. Furthermore, key questions regarding the microscopic structure of water around a small hydrophobic solute remain unanswered.

In this work, we have used a combination of classical and first-principles molecular dynamics (FPMD) simulations to probe the impact of small hydrophobic solutes on the local structure of water. In particular, we have carried out FPMD simulations of methane (CH_4) and silane (SiH_4) in water, which represent two nonpolar molecular solutes that have slightly different sizes. We also carried out a series of classical MD simulations in which the C−H bond distance, charge transfer, and pressure of the simulation cell are all systematically varied. Our simulations reveal an important interplay between solute−water and water−water interactions that govern the subtle changes in water structure around small hydrophobic solutes. Spatial distributions are found to be influenced mainly by the shape and resulting steric effects of the solute. Angular orientations and hydrogen bond networks, on the other hand, are driven by the water−water interactions at the hydrophobic solute interface. Our accurate quantum mechanical description provides a new basis with which to benchmark the reliability of classical models for the prediction of hydrophobic hydration structure. This work demonstrates that several common classical water potentials in use today (TIP4P,[20] TIP4F,[21] and TIP5P[22]) give results in good agreement with our FPMD simulations for computed radial and spatial distribution functions of water around different hydrophobic solutes. The angular orientation of the water, on the other hand, varies from one classical potential to another. In addition, the detailed hydrogen bonding network near the solute interface shows strong features in our FPMD simulations, which are absent in the classical MD results.

II. Computational Methods

A. First Principles Molecular Dynamics. In our FPMD calculations, both methane and silane are placed in a periodically repeating box with 57 water molecules. The Car−Parrinello[23] molecular dynamics approach is employed within a parallel first-principles molecular dynamics code.[24] Our approach is based on density functional theory with the Perdew−Burke−Ernzerhof generalized gradient approximation.[25] Electron−ion interactions are treated with norm conserving nonlocal pseudopotentials of the Hamann type,[26] and the Kohn−Sham orbitals are expanded in plane waves up to a kinetic energy cutoff of 85 Ryd. A time step of 0.05 fs and a fictitious electronic mass of 300 au were used for the dynamics.[27] We used cubic supercells with periodic boundary conditions and volumes that reproduce the density of water at normal conditions (L = 12.22 Å for methane−water and L = 12.37 Å for silane−water). Each simulation was started by heating the system to 600 K for 1 ps, subsequently cooling

10.1021/jp0470187 CCC: $27.50
Published on Web 09/15/2004

TABLE 1: Geometry and Potential Parameters for the Water Models

	TIP4P	TIP4F	TIP5P
q_H (e)	0.520	0.511	0.241
q_L (e)	−1.040	−1.022	−0.251
σ_O (Å)	3.15365	3.27	3.12
ϵ_O (kcal/mol)	0.1550	0.10	0.16
r_{OH} (Å)	0.9572	0.9572	0.9572
r_{OL} (Å)	0.150	0.175	0.70
θ_{HOH} (deg)	104.52	109.5	104.52
θ_{LOL} (deg)			109.47
k_{OH} [kcal/(mol Å^2)]		600.0	
k_{OL} [kcal/(mol Å^2)]		900.0	
k_{HOH} [kcal/(mol rad^2)]		75.0	
k_{HOL} [kcal/(mol rad^2)]		50.0	

TABLE 2: Geometry and Potential Parameters Used for Methane

q_C (e)	−0.240
q_H (e)	0.060
σ_C (Å)	3.50
σ_H (Å)	2.50
ϵ_C (kcal/mol)	0.0659
ϵ_H (kcal/mol)	0.0293
r_{CH} (Å)	1.0906
θ_{HCH} (deg)	109.4712
k_{CH} [kcal/(mol Å^2)]	367.0
k_{HCH} [kcal/(mol Å^2)]	35.0

to 300 K for 1 ps, and equilibrating for 1 ps before recording data under constant energy and volume conditions. A velocity scaling thermostat was used during the equilibration stage (first 3 ps) and then turned off while statistics were collected. For each solute, we performed 8 separate 9 ps (i.e., 6 ps of statistics) quantum simulations with different and uncorrelated starting configurations obtained from classical runs. The total simulation time of ∼50 ps for each solute, was confirmed with classical simulations to be sufficient for obtaining well converged averages.

We note that in our FPMD approach, the atoms are propagated with classical dynamics, i.e., Newtonian equations of motion. The inclusion of quantum effects for the protons could play a role in the simulation results. Recently, we have found that the effect of proton quantum motion in calculated structural properties such as radial distribution functions may be equivalent to increasing the ionic temperature by as much as 50−100 K for pure water at ambient conditions.[28] The explicit inclusion of proton quantum effects in our FPMD simulations is beyond the scope of the present work.

B. Classical Molecular Dynamics. In addition to the quantum simulations, we have performed a series of classical dynamics simulations for methane in water using the same number of water molecules and periodically repeating unit cell as in our quantum simulations. To represent the water in our classical simulations, we have used the TIP4P[20] and TIP5P[22] rigid water models and the TIP4F[21] flexible water model (see Table 1). In each of the simulations, the methane was described with the OPLS all-atom model[29] given in Table 2. Size effects have been examined by repeating the TIP5P simulations with a single methane solute molecule with 216 and 512 water molecules, which gave nearly identical results for the tested structural properties. All classical molecular dynamics simulations have been performed with the Tinker simulation package.[30] The simulation temperature was controlled with a weakly coupled Berendsen thermostat,[31] and molecular dynamics time steps of 0.5 and 0.25 fs were used for the rigid and flexible water simulations, respectively. Long-range electrostatic interactions were included with the particle-mesh Ewald method.[32]

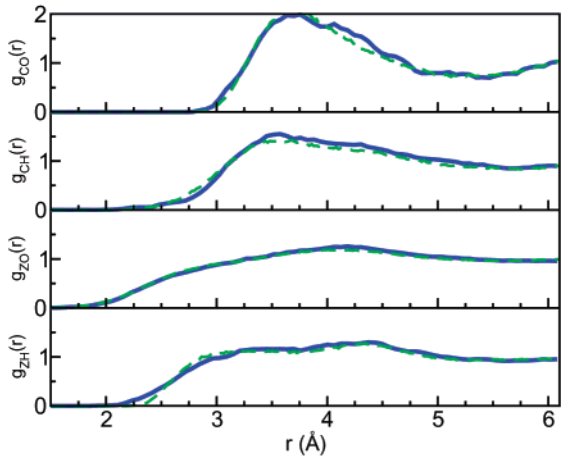

Figure 1. Radial distribution functions for FPMD (solid) and classical TIP5P (dashed) water−methane simulations. For the *y*-axis labels in this figure, the symbol "Z" is used to represent the hydrogen atoms of the methane molecule and "H" is used to represent the hydrogen atoms of the water molecules. Data are averaged over 48 (500) ps for the FPMD (TIP5P) simulations.

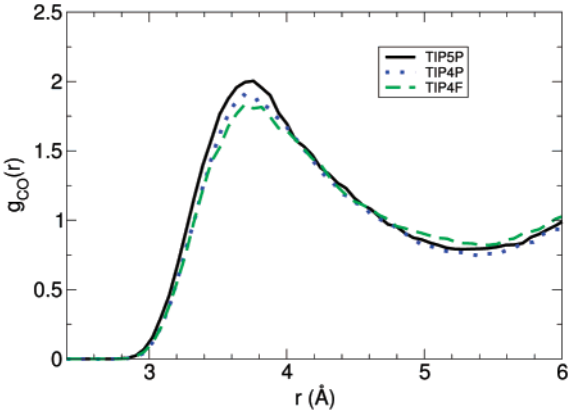

Figure 2. C−O radial distribution functions for TIP5P, TIP4P, and TIP4F classical water−methane simulations. Data are averaged over 500 ps.

III. Comparison of FPMD and Classical MD for CH_4

A. Radial Distribution Function. As shown in Figure 1, for the methane−water system, classical and quantum simulations give very similar results for computed radial distribution functions (RDFs). In the following, we refer to the solute hydrogen atoms as Z and the water hydrogen atoms as H. Both simulations have similar onsets, peak positions, and peak heights for the solute−water C−O, C−H, Z−O, and Z−H RDFs.

On the basis of the C−O RDF, the simulations find a first solvation shell centered around the solute that contains roughly 20 water molecules and is peaked at 3.7 Å (see Figure 1), in agreement with recent neutron diffraction experiments,[4,5] as well as previous classical MD simulations.[13] Note that even the shapes of the classical RDFs are in very good agreement with the FPMD simulations, with perhaps the only minor disagreement appearing at the onset of the Z−H RDF, where FPMD predicts that the water hydrogen atoms can come ∼0.2 Å closer to the methane hydrogen atoms.

If Figure 1, FPMD results are compared with the TIP5P potential. A comparison with the other classical potentials considered in this work (TIP4P and TIP4F) for the C−O RDF is shown in Figure 2. Note that the different classical potentials are in good agreement with one another for peak positions. The TIP5P potential leads to a slightly more structured C−O RDF than the TIP4P and TIP4F potentials.

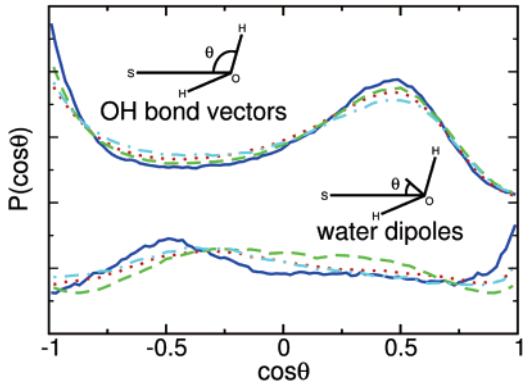

Figure 3. Distribution of tilt angles in the first solvation shell (r < 5.2 Å) of water around methane. We plot the tilt angle between the vector joining the water's oxygen to the solute and both the dipole moment vector and the O−H bond vectors of the water molecules. Classical simulation results are shown for TIP4P, TIP4F, and TIP5P potentials as dotted, dash−dotted, and dashed curves, respectively. FPMD simulation results are shown as solid curves. The O−H bond tilt angle distribution has been shifted vertically for clarity.

B. Angular Distribution Function. Despite these similarities between the FPMD and classical MD simulations for the methane−water system, there is a notable difference in the angular orientations of water molecules around the solute (see Figure 3). Our FPMD simulation shows an asymmetric distribution of the water molecules' dipole tilt angles, with enhanced probabilities near $\cos(\theta) = -0.5$ (120°) and $\cos(\theta) = 1.0$ (0°). This picture contrasts the classical TIP5P simulation results, which predict a more symmetric distribution with a broad, flat peak around $\cos(\theta) = 0$, indicating mostly random orientations of the water dipoles with respect to the solute. The TIP4P potential is in slightly better agreement with the FPMD results for the water dipole distribution; however, the TIP4P distribution of O−H bond vectors is slightly less structured than TIP5P, putting it in worse agreement when compared with FPMD. It appears that the difference in angular orientations between the classical potentials is mainly due to the impact of the potential geometry (i.e., 4-site vs 5-site) on energetically favorable configurations, as was noted previously.[33]

Although the FPMD and classical MD O−H bond vector distributions appear similar, note that the quantum distribution shows an enhancement of the peaks at +0.5 and −1.0. The classical potentials are in much better agreement with one another for the O−H bond vector than for the dipole moment vector, similar to previous observations.[33] Earlier work suggested that the alignment of the radial distribution function for the C−O and C−H first peaks as well as the Z−O and Z−H first peaks is indicative of a tangential orientational preference of the water molecules.[13] The present results confirm the observation[33] that information regarding specific orientation inferred from globally averaged properties such as radial distribution functions can be misleading.

For methane, the 120° contributions to the tilt angles derive mostly from the inner part of the first C−O solvation shell, i.e., closest to the hydrophobic interface. Conversely, in the outer part of the C−O solvation shell the small-angle peak appears while contributions to the 120° orientation are significantly lessened. This finding agrees with previous results[5] which found that the outer parts of the hydration shell give rise to small tilt angles. Our FPMD results for the dipole tilt angles of water around methane do not support previous studies that suggested a hydration structure composed of water dipole vectors tangentially oriented to the surface of the solute.[34]

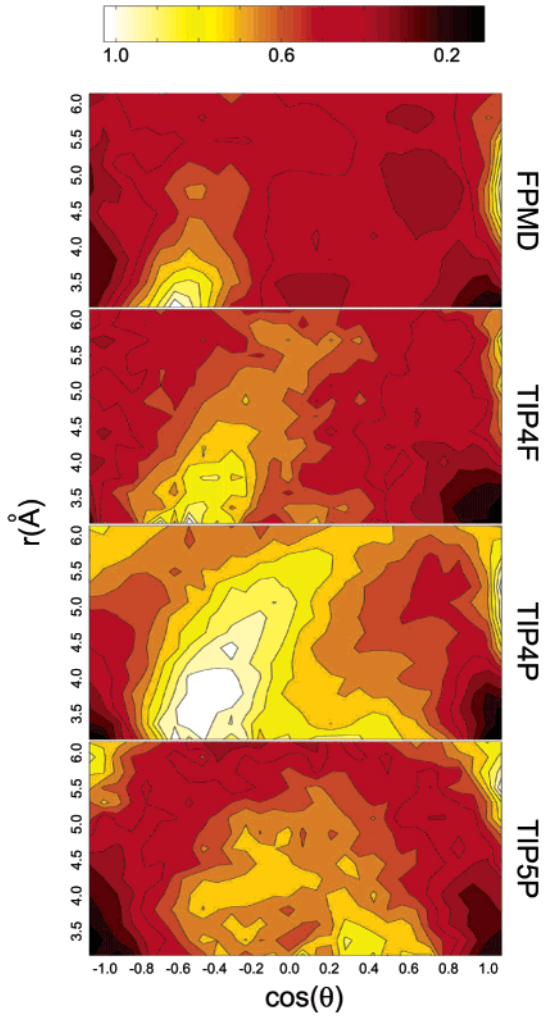

Figure 4. Distribution of tilt angles of water around methane for the FPMD and classical (TIP4P, TIP4F, and TIP5P potentials) simulations. Results are shown as a function of the C−O distance.

In Figure 4, we show contour plots of the water dipole tilt angle distribution as a function of distance from the solute center, to illustrate the differences between the simulations in more detail. Near the interface, the TIP4P distribution has a strong peak at $\cos(\theta) = -0.4$ and less structure toward the outer edge of the first solvation shell. In contrast, near the interface the TIP5P distribution has a peak at $\cos(\theta) = -0.4$ but also a significant contribution at $\cos(\theta) = +0.4$ and values in between. Further, unlike TIP4P, the TIP5P distribution shows a peak centered around $\cos(\theta) = 0.0$ for $r_{CO} \sim 4.0-4.5$ Å, indicating a preference for tangential orientation of the water molecules at the outer edge of the first solvation shell. Another difference occurs at the first minimum in $g_{CO}(r)$; both potentials show a peak in the tilt angle distribution at $\cos(\theta) = 1.0$, but the TIP5P potential leads to a second peak at $\cos(\theta) = -1.0$, which is not the case for TIP4P. Note that both the TIP4P and TIP5P classical potentials differ from the FPMD results throughout the entire first solvation shell. The structure in the FPMD tilt distribution is more localized: FPMD shows two distinct peaks, one at $\cos(\theta) = -0.6$ near the hydrophobic interface and one at $\cos(\theta) = 1.0$ further away from the interface, whereas in the classical simulations the structure is more broadly distributed throughout the first solvation shell.

The tilt angle distribution for the TIP4F flexible water model considered in this work is also shown in Figure 4. In contrast to the two rigid models, TIP4F shows better agreement with

the FPMD results. The flexibility tends to lessen the extent to which the peak at −0.5 penetrates from the interface out into the first solvation shell; for TIP4P this region extends to ∼5.0 Å whereas for TIP4F it reaches only ∼4.0 Å, as does the FPMD simulation result.

Recent simulations of pure water with the TIP5P potential have found that when long range interactions are treated accurately (e.g., with Ewald summations) the improved agreement with experiment of TIP5P over TIP4P is diminished.[35] For example, the temperature of maximum density is known to shift from 4 °C at 1 atm when a spherical cutoff is used, to 11 °C with Ewald summation[35] (the corresponding experimental value is 4 °C[36]). In addition, previous classical simulations of hydrophobic hydration have found that the presence of a hydrophobic solute is felt at long distances due to its ability to alter the electrostatic charge distribution of the liquid.[37] Inspection of Figure 4 reveals that the TIP4P potential results in a tilt angle distribution that is in better qualitative agreement with FPMD than with TIP5P, which may indicate that TIP4P provides a more robust potential as compared to TIP5P when long range interactions are accurately taken into account.

IV. Comparison of Methane and Silane in FPMD Simulations

There is a limited understanding of how differences between various hydrophobic solutes can result in differences in the microscopic structure of the water surrounding the solute.[33,38−40] In particular, previous theoretical investigations have examined how the size of the solute influences the structure of the first solvation shell by representing the solute with a hard sphere.[33] In the small solute limit, these simple models indicate that there is only a weak dependence on the orientation of first solvation shell water molecules with the size of a hydrophobic solute. To examine if a similar trend exists when more realistic models are considered, we have performed FPMD simulations of silane in water. We have chosen silane because of its similarity in bonding character (sp^3), and its moderate difference in size (silane is approximately the same size as a Xe atom in solution). In addition, there are small differences in the electronegativities of silicon and carbon that result in a small amount of charge transfer away from the silicon atom rather than toward, as with carbon.

Interestingly, the single property we find that differs between classical and quantum simulations for CH_4, namely the orientation of water around the solute, is one of the few properties that both CH_4 and SiH_4 share in common within the FPMD simulations. Figure 5 shows that, as in the case of methane, the angular distribution of water dipoles around silane is asymmetric, with enhancements at ∼120° orientations near the hydrophobic interface and at small angles toward the outer edge of the first solvation shell.

To probe the detailed structure of liquids, spatial distribution functions (SDF) have become a powerful analysis tool that provides three-dimensional maps representing local atomic densities.[41,42] The SDFs are computed as a density distribution of the water molecule's oxygen atom position relative to a fixed orientation of the solute. The lobes of our calculated SDF for the methane−water system are well-aligned with the peaks in the RDF measured by neutron diffraction.[6,7] In the case of methane, both the classical and quantum simulations find nearly random spatial arrangements of water within the first solvation shell, implying much smaller water−solute interactions at the interface as compared to water−water interactions. In accord with current views of the hydrophobic hydration of small

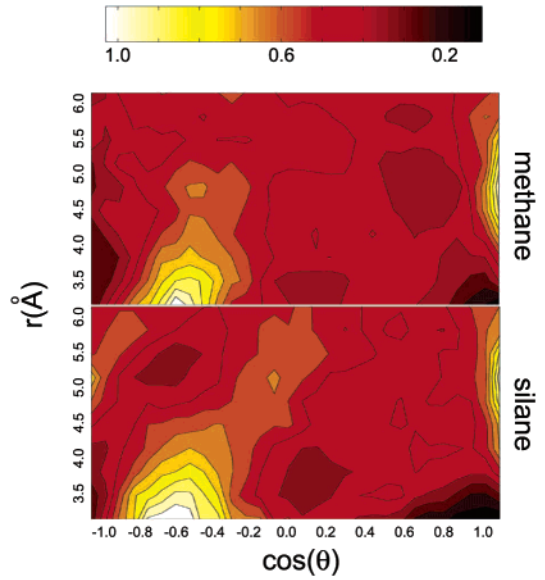

Figure 5. Distribution of tilt angles of water around methane and silane for the FPMD simulations. Results are shown as a function of the C−O and Si−O distances.

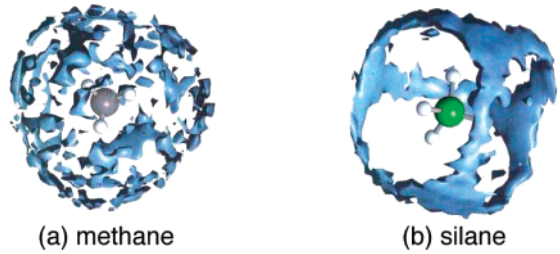

Figure 6. Spatial distribution functions for water−methane and water−silane simulations. In each case, the same threshold is plotted for the local density of oxygen averaged over symmetric orientations of the solute.

solutes,[43] the spatial ordering of water around methane appears to be governed predominantly by the water−water hydrogen bonding.

In sharp contrast to the random SDF of water around methane, the spatial distribution around silane exhibits a strong angular preference. In Figure 6, both distribution functions are plotted using the same threshold (10% of the water in the first solvation shell, i.e., ∼2 water molecules). Note the preference of water to avoid Si−H bond axes and collect in regions between any 3 hydrogen atoms of the silane molecule. As one increases the plotting threshold, the same kind of distribution is in fact also observed around methane, although it is much weaker (i.e., barely visible in such plots) than for silane.

One possible explanation for the difference between the methane and silane SDFs is that the distributions of water around the solutes are actually similar, but the rotational correlation time of methane in water is too short to observe the solvation shell's structure from the perspective of the solute reference frame. To examine the rotational dynamics, we have compared the different solutes by computing the single-molecule orientational relaxation function[44] and assuming a Debye-type relaxation. CH_4 was found to have a rotational correlation time that is approximately 5 times shorter than that of SiH_4. However, the same randomized SDF around methane is observed if one changes the reference frame to be defined by the simulation cell rather than the solute, making the faster rotational correlation time of methane an unlikely explanation. It is, therefore, reasonable to assume that the distributions of water around silane

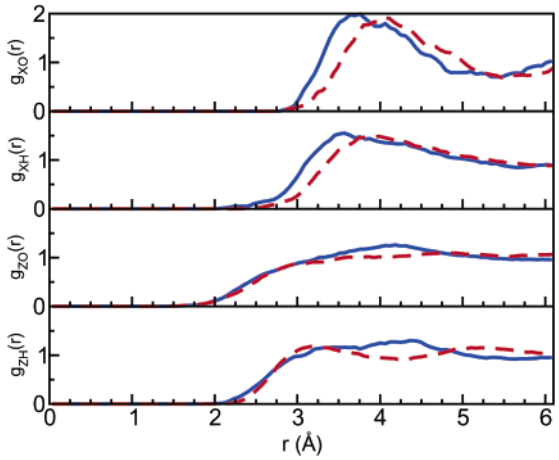

Figure 7. Radial distribution functions for FPMD water−methane (blue, solid) and water−silane (red, dashed) simulations. For the *y*-axis labels in this figure, "XZ_4" is used to represent atom species of the solute, either SiH_4 or CH_4. Data are averaged over 48 ps for each case.

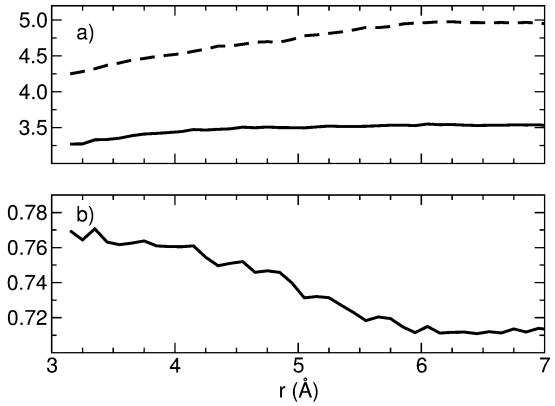

Figure 8. Average number of hydrogen bonds and nearest neighbors as a function of the distance from the center of the methane solute in the TIP4F/methane simulation. In (a) the solid line corresponds to the average number of hydrogen bonds, and the dashed line to the average number of nearest neighbors. In (b) the solid line corresponds to the average number of hydrogen bonds per nearest neighbors.

and methane correspond to different spatial ordering of water around the solutes.

Another explanation for the structural difference in water near methane and silane is that it is driven by steric effects. This would imply that the water molecules are able to fill the volume between a given set of three neighboring hydrogen atoms more easily for silane than for methane. The surface area of the equilateral triangle formed by three hydrogen atoms is 2.8 $Å^2$ for silane compared with 1.5 $Å^2$ for methane, and the volume contained in the tetrahedron formed by connecting this triangle to the central atom is more than 2.5 times larger in silane than methane. Thus, an increase in bond length by about one-third may lead to an "opening" large enough from the perspective of the water, to create a strong structural change in the vicinity of the hydrophobic interface. This space-filling argument may appear rather straightforward; however, it is particularly interesting that, given the large structural changes in the positions of the oxygen atoms at the interface, the more subtle angular distributions of the water molecules are not affected. As such, we can suppose that a significant (steric) interaction between the silane molecule and the surrounding water drives spatial changes, whereas the hydrogen bonding interactions, which dictate relative orientational ordering between waters, are largely unaffected.

Figure 7 shows a comparison between RDFs of CH_4 and SiH_4 computed in our FPMD simulations. The Si−O and Si-Z distributions are similar but shifted out by 0.4 Å compared to methane−water, in line with what one might expect from the fact that the Si-Z bond distance in silane is 0.4 Å larger than the C−Z distance in methane. On the other hand, we find that the radial distributions involving the hydrogen atoms of the solutes, Z−O and Z−H (lower two panels of Figure 7), are different between the two hydrophobic molecules. Yet, these differences appear to be compatible with the difference observed between the SDFs. For example, the first peak at 3.2 Å in the O−Z RDF is consistent with an oxygen atom placed in the pocket between the hydrogen atoms (as indicated by the SDF) at roughly a distance of 4.1 Å from silicon, in line with the first O−Si RDF peak. Similarly, the broad distribution in the O−Z RDF is consistent with the random SDF observed at the methane−water interface.

Neutron diffraction experiments have shown that water can form a loosely ordered, cage-like structure around hydrophobic solutes.[6] Furthermore, recent vibrational sum spectroscopy measurements[8] suggested that hydrogen bonding at the hydrophobic interface might be weaker than expected. A geometric analysis of the number of hydrogen bonds (a maximum O−O separation of 3.5 Å and a minimum O−H−O angle of 140°) as a function of distance from the solute center appears to support this observation. As shown in Figure 8a obtained from the TIP4F simulation of methane in water, the average number of hydrogen bonds gradually decreases within the first solvation shell. However, it is interesting to note that the number of nearest neighbors (defined by the same maximum O−O separation of 3.5 Å) decreases at a faster rate, which results in an increase in the ratio of hydrogen bonds to nearest neighbors near the solute−water interface (see Figure 8b). A similar increase is found in the FPMD simulation of methane in water. As was noted in ref 33, this finding supports the notion that the orientation of water molecules near the solute−water interface is largely controlled by water−water interactions that attempt to maintain the hydrogen bond network. In addition, these results indicate that the depleted density around the solute leads to a more ice-like hydrogen bonding region rather than gaslike behavior.

To further investigate the influence of methane and silane on the hydrogen bond network, we have enumerated the number and size of polygon rings formed by nonshort-circuited hydrogen bond waters within the first solvation shell of the solutes.[45,46] Similar to the hydrogen bond ring distributions that are found within the first solvation shell of methane hydrates, we find that both silane and methane have pentagonal and hexagonal rings in a ratio of 4:1 (Figure 9), although the total number of hexagons and pentagons around silane is smaller than in methane by a factor of 2. This strong presence of pentagonal rings is consistent with clathrate-like behavior, in qualitative agreement with ref 46, although here we employ a geometric rather than energetic hydrogen bond criterion.

As shown in Figure 9, there is a notable increase in the number of heptagonal rings in the silane case that does not occur in the methane simulation. We have recomputed SDFs around silane by only including oxygen atoms that are part of either pentagonal or heptagonal rings. Within the limited simulation time of the FPMD simulations, the SDF composed of only heptagonal rings appears to exhibit the same structural features seen for silane in Figure 6b, whereas no discernible structure is found in the SDF composed of only pentagon rings. This result supports our earlier postulate that the structural differences

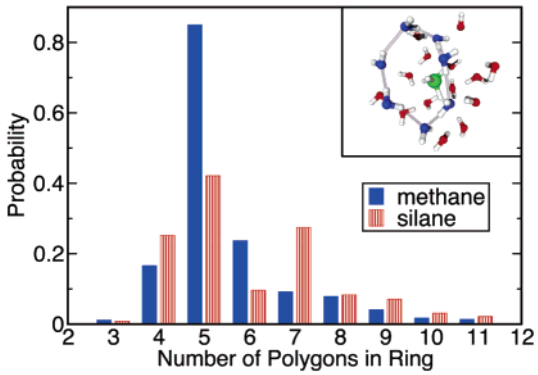

Figure 9. Distributions of hydrogen-bonded pathways for the first solvation shell of methane and silane as obtained in FPMD. We define a hydrogen bond geometrically with a maximum O−O separation of 3.5 Å and a minimum O−H−O angle of 140°. The number of polygons corresponds to the number of hydrogen bonds that make up a given closed ring. The inset shows a snapshot of the first solvation shell of water around silane; an example of a heptagonal ring located around one of the Si−H axes is shown in blue.

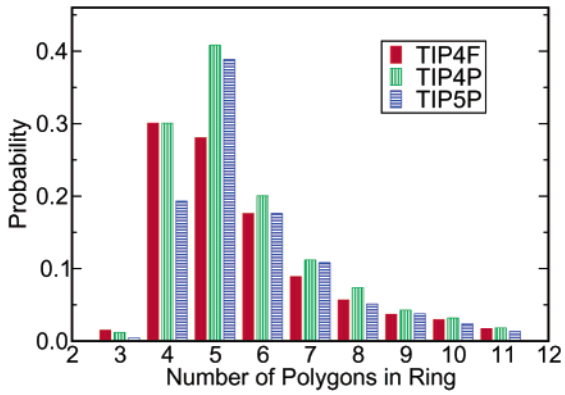

Figure 10. Distributions of hydrogen-bonded pathways for the first solvation shell of methane computed using three different classical potentials. We define a hydrogen bond geometrically with a maximum O−O separation of 3.5 Å and a minimum O−H−O angle of 140°. The number of polygons corresponds to the number of hydrogen bonds that make up a given closed ring.

observed in the SDFs influence the hydrogen bonding network, whereas the water−water interactions, which dominate angular orientations, are unchanged.

We have also computed the same hydrogen-bonded ring statistics for the first solvation shell around methane using the TIP4P, TIP4F, and TIP5P classical potentials, as shown in Figure 10. In all three cases the relative number of hexagonal rings is much greater than in our FPMD simulations, with ratios of pentagons to hexagons of ∼2:1 or less, rather than 4:1. Also, note that both the rigid and flexible TIP4 potentials lead to a strong enhancement of the number of 4-fold rings compared to the TIP5P potential. In the case of the flexible TIP4F potential, the number of 4-fold rings is actually larger than the number of pentagonal rings.

V. Classical Simulations of Pressure and Bond Length Variations

Our results thus far are indicative of a steric interaction that drives the structure and hydrogen bonding of water near a small hydrophobic solute, whereas the strong water−water interactions drive orientational order. It is worthwhile to carry out a number of "test" simulations which, even if not necessarily physical, allow us to probe more closely the influence of steric effects on the structural properties of water. To this end, we have

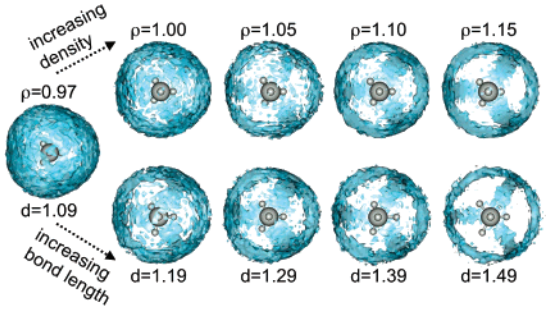

Figure 11. Spatial distribution functions for a series of classical methane−water simulations with increasing density (g/mL) and increasing C−H bond length (Å).

performed a series of solute−water simulations using classical potentials, wherein we are able to test a number of different variations on the solute and its environment. Specifically, we performed a set of methane−water calculations in which both the density (or pressure) of the system and the C−H bond length are systematically increased. For ambient conditions, we use the average density ($\rho_o = 0.97$ g/mL) given by a 2 ns constant-pressure simulation, and the C−H bond length ($d_o = 1.09$ Å) is set to the experimentally measured value (i.e., the same methane−water configuration used to compare with FPMD results in section 3). We carried out eight additional 0.5 ns simulations with densities $\rho = 1.00$, $\rho = 1.05$, $\rho = 1.10$, and $\rho = 1.15$ g/mL at $d = d_o$, and bond lengths $d = 1.19$, $d = 1.29$, $d = 1.39$, and $d = 1.49$ Å at $\rho = \rho_o$.

Calculated SDFs from these simulations are shown in Figure 11. As the density of the system is progressively increased by decreasing the volume of the simulation cell, note that the water molecules are pushed into the region between the hydrogen atoms of the methane molecule. As observed in previous classical simulations, at high enough pressures the water overcomes steric effects to form a structured shape around the solute. The bottom part of Figure 11 shows calculated SDFs for fixed-volume runs in which the C−Z bond length was increased systematically in 0.1 Å increments. As the bond length is increased, a similar effect is observed on the SDF as for the case of increasing the density. The largest C−Z bond length in our calculations ($d = 1.49$ Å) is the same as the Si−Z distance in silane, and the resulting SDF is very similar to the silane−water SDF in our FPMD calculations. Thus, the same enhancement of the structure of water around methane is obtained either by (i) increasing the accessible interstitial volume between solute hydrogen atoms via increased C−Z bond length, or (ii) by forcing the water into the available volume region through the application of pressure to the system. Furthermore, we speculate that the increase in structure seen in Figure 11 may be related to the tendency of small hydrophobic solutes such as methane to disperse rather than cluster together as pressure is applied.[47,48]

Both methane and silane contain internal dipoles set up by the charge transfers that symmetrically cancel, although close enough to the interface there may be local effects. In methane, about 0.1 electron per H atoms is transferred to the carbon atom, whereas in silane about 0.1 electron per H atom is transferred away from the silicon atom. Yet, it is unlikely that this reversal of charge transfer plays a significant role for structural properties since the spatial distribution around a solute with the silane bond length but the methane charge transfer is able to reproduce the FPMD silane−water structure so well. As a further test, we carried out two additional classical simulations using the methane and silane bond lengths, but with the charge transfer in the potential set as equal and opposite of that in the standard

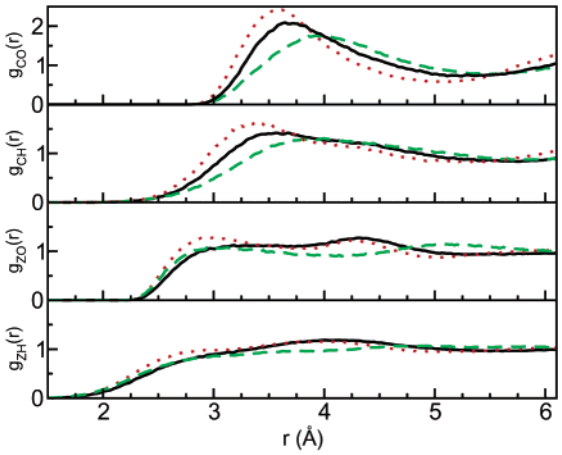

Figure 12. Radial distribution functions for a series of classical simulations. The black solid lines correspond to the ambient methane−water system ($\rho = 0.97$, $d = 1.09$), red dotted lines correspond to the largest density ($\rho = 1.15$, $d = 1.09$) simulation, and green dashed lines correspond to the largest C−H bond distance ($\rho = 0.97$, $d = 1.49$). For the *y*-axis labels in this figure, the symbol "Z" is used to represent the hydrogen atoms of the methane molecule and "H" is used to represent the hydrogen atoms of the water molecules.

methane potential. The results were found to be indistinguishable from the same simulations with the charge transfer reversed. It is, of course, possible that local charge fluctuations within the solute could affect electronic properties of the system such as the shape of the eigenstates near the Fermi energy, which would impact, e.g., the optical gap. However, the results presented here lend further credence to the notion that structural differences in the water around these small hydrophobic solutes are largely due to steric effects.

In Figure 12, it is shown that the RDFs for these classical simulations are sensitive to increases in both the pressure and C−Z distance. For the C−O and C−H distributions, increasing the pressure results in a shift in and slightly larger amplitude of the first peak, whereas increasing the C−Z bond length results in a shift outward and lower amplitude of the first peak. These results are to be expected because the higher pressure reduces the exclusion volume around the nonpolar solute whereas the longer bond length increases this volume.

For the Z−O distribution, the pressure increase results in the formation of a small peak at $r = 2.9$ Å, indicative of the water's ability to come closer to the region between the hydrogen atoms of the solute. The second peak is largely unaffected. On the other hand, with increasing C−Z bond length, the second peak is shifted out by 0.7 Å whereas the first peak is only slightly changed.

The ring statistics for the large pressure and longer C−Z bond length simulations are shown in Figure 13. In these classical simulations, the main difference upon increasing the C−Z bond length of the solute from the methane C−Z distance ($d = 1.09$ Å) to the silane Si−Z distance ($d = 1.49$ Å) is a decrease in the number of pentagonal rings in the first solvation shell. On the other hand, keeping the bond length the same but increasing pressure leads to an increase in the number of pentagonal rings. Four- and six-member rings are also more abundant in the high-pressure simulation. Note that there is no enhancement of the probability of finding 7-fold rings around the solute with a longer C−H bond, as was found in our FPMD simulations of SiH_4. This result is perhaps expected, on the basis of the other differences observed here between classical and quantum MD simulations in describing the subtleties of the hydrogen bonding network.

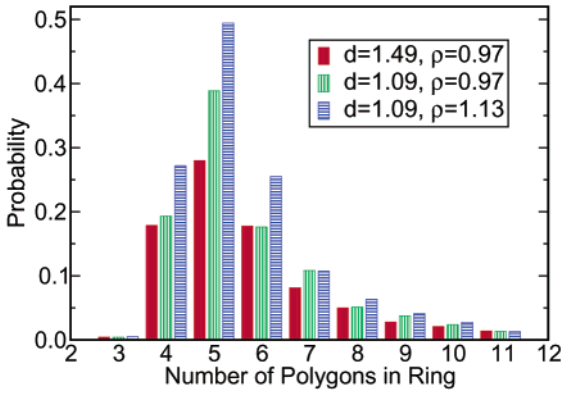

Figure 13. Distributions of hydrogen-bonded pathways for the first solvation shell of methane computed from TIP5P simulations with high density and large C−H bond length, compared with ambient conditions. We define a hydrogen bond geometrically with a maximum O−O separation of 3.5 Å and a minimum O−H−O angle of 140°. The number of polygons corresponds to the number of hydrogen bonds that make up a given closed ring.

Combining the results of these pressure and solute size simulations leads to an interesting contrast. Both increased solute size and increased pressure leads to the same spatial structuring, as observed in the SDF. However, the *type* of structure is clearly different, as observed in the ring statistics as well as the RDFs.

VI. Conclusions

The temperature dependence of the solubility of nonpolar solutes is typically explained as a competition between entropic and enthalpic contributions at the macroscopic scale. Yet, it is the unique properties of water around hydrophobic solutes at the *microscopic* scale that ultimately drives these interesting properties. To directly investigate the structural nature of hydrophobic hydration, we have carried out a series of molecular dynamics simulations of small hydrophobic solutes in water at ambient conditions, including the use of both classical as well as first-principle simulation techniques.

Though previous work has found only small differences in the structure of water in the small hydrophobic solute limit,[33] our work illustrates that there is a dramatic steric effect of the specific size and shape of the small solute on the spatial distribution of water at the water−solute interface. In addition, we have shown that the angular orientation of the water molecules is insensitive to this spatial structure and is dominated by the strong water−water interactions. Our results suggest that the hydrogen bonding network is preserved around the solute, possibly leading to ice-like structure in the depleted water region around small nonpolar solutes.

A direct comparison with our FPMD results allows us to benchmark the accuracy of three different classical potentials used to simulate the same systems. We find that the overall hydrophobic hydration structure is well-described by the tested classical potentials. However, subtle hydrogen-bonding effects may pose a challenge to empirical-based models. In particular, angular distributions and details regarding the hydrogen-bonded network of waters around the hydrophobic solute are quite different between the different classical potentials. Despite the fact that all of the properties that we have computed with FPMD can be well represented by at least one of the classical simulation results, there is not a single classical model that is capable of reproducing all of the properties found within FPMD simultaneously.

The results of this work present an exciting challenge to experiments: to probe the detailed structural differences of water

around varying hydrophobic solutes. A number of systems other than CH_4 and SiH_4 could be used to confirm the picture presented here; for example, carbon tetrachloride may behave in a manner similar to SiH_4 but different from CH_4. New experiments are continuing to overcome the difficulties associated with selectively examining water molecules near a hydrophobic solute,[5,49,50] and we believe that further understanding of these structural differences will be elucidated by a combination of such experiments and accurate simulations.

Acknowledgment. We thank David Chandler, Alan Soper, and Lawrence Pratt for useful discussions. This work was performed under the auspices of the U.S. Department of Energy by the University of California Lawrence Livermore National Laboratory under contract No. W-7405-Eng-48.

References and Notes

(1) Kauzmann, W. In *The Mechanism of Enzyme Action*; McElroy, W. D.; Glass, B., Eds.; The Johns Hopkins Press: Baltimore, MD, 1954.
(2) Englezos, P. *Ind. Eng. Chem. Res.* **1993**, *32*, 1251.
(3) Kauzmann, W. *Nature* **1987**, *325*, 763.
(4) Jong, P. H. K. D.; Wilson, J. E.; Neilson, G. W.; Buckingham, A. D. *Mol. Phys.* **1997**, *91*, 99.
(5) Koh, C. A.; Wisbey, R. P.; Wu, X.; Westacott, R. E.; Soper, A. K. *J. Chem. Phys.* **2000**, *113*, 6390.
(6) Soper, A. K.; Finney, J. L. *Phys. Rev. Lett.* **1993**, *71*, 4346.
(7) Bowron, D. T.; Filipponi, A.; Roberts, M. A.; Finney, J. L. *Phys. Rev. Lett.* **1998**, *81*, 4164.
(8) Scatena, L. F.; Brown, M. G.; Richmond, G. L. *Science* **2001**, *292*, 908.
(9) Steitz, R.; Gutberlet, T.; Hauss, T.; Klösgen, B.; Krastev, R.; Schemmel, S.; Simonsen, A. C.; Findenegg, G. H. *Langmuir* **2003**, *19*, 2409.
(10) Jensen, T. R.; Jensen, M. O.; Reitzel, N.; Balashev, K.; Peters, G. H.; Kjaer, K.; Bjørnholm, T. *Phys. Rev. Lett.* **2003**, *90*, 086101.
(11) Pratt, L. R. *Annu. Rev. Phys. Chem.* **2002**, *53*, 409.
(12) Head-Gordon, T. *J. Am. Chem. Soc.* **1995**, *117*, 501.
(13) Guillot, B.; Guissani, Y.; Bratos, S. *J. Chem. Phys.* **1991**, *95*, 3643.
(14) Lee, S. H.; Rossky, P. J. *J. Chem. Phys.* **1993**, *100*, 3334.
(15) Cui, Q.; Smith, V. H. *J. Chem. Phys.* **2000**, *113*, 10240.
(16) Gordillo, M. C.; Marti, J. *J. Chem. Phys.* **2002**, *117*, 3425.
(17) Hernández-Coboz, J.; Mackie, A. D.; Vega, L. F. *J. Chem. Phys.* **2001**, *114*, 7527.
(18) Pratt, L.; Pohorille, A. *Chem. Rev.* **2002**, *102*, 2671.
(19) Jorgensen, W. L.; Blake, J. F.; Buckner, J. K. *Chem. Phys.* **1989**, *129*, 193.
(20) Jorgensen, W. L.; Madura, J. D. *Mol. Phys.* **1985**, *56*, 1381.
(21) Mahoney, M. W.; Jorgensen, W. L. *J. Chem. Phys.* **2001**, *115*, 10758.
(22) Mahoney, M. W.; Jorgensen, W. L. *J. Chem. Phys.* **2000**, *112*, 8910.
(23) Car, R.; Parrinello, M. *Phys. Rev. Lett.* **1985**, *55*, 2471−2474.
(24) Gygi, F. GP 1.24.0: A general ab initio molecular dynamics program. Lawrence Livermore National Laboratory, 2003.
(25) Perdew, J. P.; Burke, K.; Ernzerhof, M. *Phys. Rev. Lett.* **1996**, *77*, 3865−3868.
(26) Hamann, D. R. *Phys. Rev. B* **1997**, *55*, 10157−10160.
(27) Grossman, J. C.; Schwegler, E.; Draeger, E. W.; Gygi, F.; Galli, G. *J. Chem. Phys.* **2004**, *120*, 300.
(28) Schwegler, E.; Grossman, J. C.; Gygi, F.; Galli, G. *J. Chem. Phys.* **2004**, in press.
(29) Kaminski, G.; Duffy, E. M.; Matsui, T.; Jorgensen, W. L. *J. Phys. Chem.* **1994**, *98*, 13077.
(30) Ponder, J. W.; Rubenstein, S.; Kundrot, C.; Huston, S.; Dudek, M.; Kong, Y.; Hart, R.; Hodsdon, M.; Pappu, R.; Mooij, W.; Loeffler, G. "TINKER: Software Tools for Molecular Design, Version 3.9", Washington University, St. Louis, MO.
(31) Berendsen, H. J. C.; Postma, J. P. M.; van Gunsteren, W. F.; DiNola, A.; Haak, J. R. *J. Chem. Phys.* **1984**, *81*, 3684.
(32) Darden, T.; York, D.; Pedersen, L. *J. Chem. Phys.* **1993**, *98*, 10089.
(33) Předota, M.; Nezbeda, I. *Mol. Phys.* **1999**, *96*, 1237.
(34) R, L. M.; Buckingham, A. D.; Skipper, N. T. *J. Chem. Soc., Faraday Trans.* **1997**, *93*, 2263.
(35) Lísal, M.; Kolafa, J.; Nezbeda, I. *J. Chem. Phys.* **2002**, *117*, 8892.
(36) Sato, H.; Uematsu, M.; Watanabe, K.; Saul, A.; Wagner, W. *J. Phys. Chem. Ref. Data* **1988**, *17*, 1439.
(37) Fois, E.; Gamba, A.; Redaelli, C. *J. Chem. Phys.* **1999**, *110*, 1025.
(38) Lum, K.; Chandler, D.; Weeks, J. D. *J. Phys. Chem. B* **1999**, *103*, 4570.
(39) Stillinger, F. H. *J. Solut. Chem.* **1973**, *2*, 141.
(40) Předota, M.; Cummings, P. T. I. N. *Mol. Phys.* **2002**, *100*, 2189.
(41) Svishchev, I. M.; Kusalik, P. G. *J. Chem. Phys.* **1993**, *99*, 3049.
(42) Soper, A. K.; Ricci, M. A. *Phys. Rev. Lett.* **2000**, *84*, 2881.
(43) Chandler, D. *Nature* **2002**, *417*, 491.
(44) Ohmine, I. *J. Phys. Chem.* **1995**, *99*, 6767.
(45) Rahman, A.; Stillinger, F. H. *J. Am. Chem. Soc.* **1973**, *92*, 7943.
(46) Head-Gordon, T. *Proc. Natl. Acad. Sci. U.S.A.* **1995**, *92*, 8308.
(47) Wallqvist, A. *J. Chem. Phys.* **1992**, *96*, 1655.
(48) Payne, V. A.; Matubayasi, N.; Murphy, L. R.; Levy, R. M. *J. Phys. Chem. B* **1997**, *101*, 2054.
(49) Hummer, G.; Rasalah, J.; Noworyta, J. P. *Nature* **2001**, *414*, 188.
(50) Dixit, S. J. C.; Poon, W. C. K.; Finney, J. L.; Soper, A. K. *Nature* **2002**, *416*, 829.